Arccosine Vector Field Guidance for Curvilinear Path Following of UAVs

Sayantan Pal[1] and Sikha Hota[2]

Abstract— **This paper presents a vector field (VF) guidance strategy for smooth and feasible curvilinear path following of unmanned aerial vehicles (UAVs). The proposed approach defines the desired course angle as an arccosine function of the tracking error relative to the desired path. Numerical simulations with various curvilinear paths show the robustness of the proposed approach under steady wind conditions. Comparative analysis against existing guidance algorithms highlights the effectiveness and improved control efficiency of the proposed method. Experimental results further demonstrate the practical applicability of the proposed guidance law in real-world environments.**

Index Terms- Path following; Vector field guidance; Unmanned Aerial Vehicles; Sliding mode control.

I. INTRODUCTION

Unmanned Aerial Vehicles (UAVs) have found widespread applications across diverse domains, including disaster management, surveillance, search and rescue, aerial photography, and package delivery. In most of these applications, autonomous operation is essential, requiring the UAV to accurately follow a predefined trajectory. The desired paths are not limited to straight-line segments; instead, they often consist of curved geometries dictated by mission requirements and environmental constraints.

Numerous path-following strategies have been extensively studied in the literature, including Virtual Target Point (VTP)-based guidance laws, control-based approaches, and Vector Field (VF)-based guidance methods. Among VTP-based guidance laws, notable examples include the Carrot-chasing algorithm [1], Pure Pursuit [2], Line-of-Sight (LOS) guidance [3], Nonlinear Guidance Law (NLGL) [4], and Trajectory Shaping guidance [5]. In the Carrot-chasing algorithm, a virtual target point (referred to as the "carrot") is placed on the desired path, and the UAV continuously pursues this point, resulting in path convergence. The LOS guidance law steers the UAV toward the line-of-sight direction of a virtual target located on the path. Similarly, NLGL employs a virtual target positioned ahead of the UAV at a constant look-ahead distance, enabling smooth path-following behavior. The Trajectory Shaping guidance law represents another VTP-based approach that achieves faster convergence compared to the Pure Pursuit method.

In addition to VTP-based methods, several control-based strategies have been proposed to address the path-following problem. A sliding mode controller (SMC)-based guidance approach was presented in [6] to regulate lateral tracking error, while [7] combined SMC with backstepping for UAV path tracking. An adaptive Linear Quadratic Regulator (LQR) controller was introduced in [8] to handle the path following problem under wind disturbances. Furthermore, a Lyapunov-based fixed-time controller was proposed in [9] to ensure convergence to the desired path within a fixed time. A comprehensive review of UAV path-following techniques is presented in [10], where VF-based approaches are shown to provide superior path-following accuracy compared to other guidance strategies.

Vector Field (VF) guidance is widely recognized as an effective path-following approach due to its superior performance in achieving accurate and smooth convergence to the desired path. The fundamental principle of VF guidance lies in constructing a vector field that prescribes the desired direction of motion at each point in the state space; by aligning its velocity with this field, the UAV asymptotically converges to the path. Based on this principle, vector fields for straight-line and circular path following were developed in [11], where asymptotic convergence in the presence of wind disturbances was established. This framework was later extended to general curved paths in [12]. To address unknown wind disturbances, an adaptive VF guidance scheme was proposed in [13]. Furthermore, the work in [11] was extended in [14] to incorporate minimum turn radius constraints of UAVs. An alternative class of VF guidance methods is the Lyapunov Vector Field (LVF) approach, originally proposed in [15] for standoff target tracking. This approach was further extended to waypoint-following missions through switching between circular VFs [16]. A curvature-constrained LVF guidance law was introduced in [17], demonstrating improved convergence performance compared to [15]. Subsequently, enhanced LVF-based methods have been developed, such as [18], which achieves faster convergence relative to earlier LVF approaches. In [19], an arcsine-based VF guidance law was proposed for path-following applications. More recently, an arccosine-based VF guidance law was introduced in [20] for straight-line and circular path following in the presence of wind disturbances while incorporating minimum turn radius constraints of the UAV. The approach in [20] demonstrates faster convergence compared to [19] under identical minimum turn radius constraints. However, these formulations are primarily limited to straight-line and circular trajectories.

To extend the applicability of our previous work in [20], this paper proposes a VF guidance framework for general

[1]Sayantan Pal, Ph.D. Scholar, Department of Aerospace Engineering, Indian Institute of Technology Kharagpur 721302, India `sayantanmech94@kgpian.iitkgp.ac.in`

[2]Sikha Hota, Associate Professor, Department of Aerospace Engineering, Indian Institute of Technology Kharagpur 721302, India. `sikhahota@aero.iitkgp.ac.in`

curvilinear path following in the presence of wind disturbances. The proposed approach generalizes the arccosine-based desired vector field to curvilinear paths. An enhanced formulation of the commanded course angle is developed using a sliding-mode-based control law, resulting in smoother transients and improved convergence. The proposed method is validated through real-world trajectory tracking experiments.

II. PROBLEM STATEMENT

The problem is to develop a VF-based guidance strategy for following general curvilinear paths in the presence of steady wind disturbances. The UAV is modeled as a point-mass nonholonomic vehicle operating at a constant altitude and constant airspeed v_a, resulting in planar motion. Let the position of the UAV in the inertial frame be denoted by $P(x,y)$, and its heading angle by ψ_a. In the absence of wind disturbances, the kinematic equations of motion are given by

$$\begin{aligned} \dot{x} &= v_a \cos\psi_a \\ \dot{y} &= v_a \sin\psi_a \end{aligned} \tag{1}$$

In the presence of wind disturbances, the ground velocity vector differs from the air relative velocity vector. Using the wind triangle shown in Fig. 1, the kinematic equations can be expressed as

$$\begin{aligned} \dot{x} &= v_g \cos\chi = v_a \cos\psi_a + w_x \\ \dot{y} &= v_g \sin\chi = v_a \sin\psi_a + w_y \end{aligned} \tag{2}$$

where χ denotes the course angle, v_g is the ground speed,

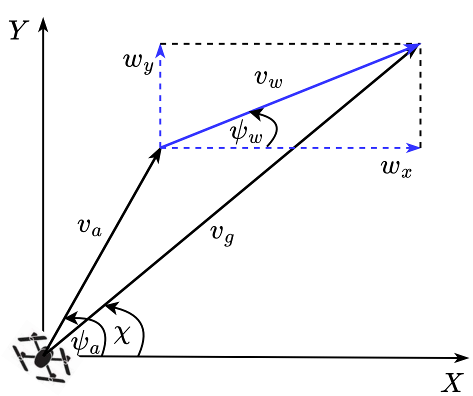

Fig. 1: Schematic representation of Wind triangle

and (w_x, w_y) represents the wind velocity components along the x and y directions, respectively. The geometric configuration of the curvilinear path-following problem is illustrated in Fig. 2. To facilitate guidance design, a first-order model of the course angle is considered, given by

$$\dot{\chi} = \alpha(\chi_c - \chi) \tag{3}$$

where, χ_c is the commanded course angle, and α is a positive constant.

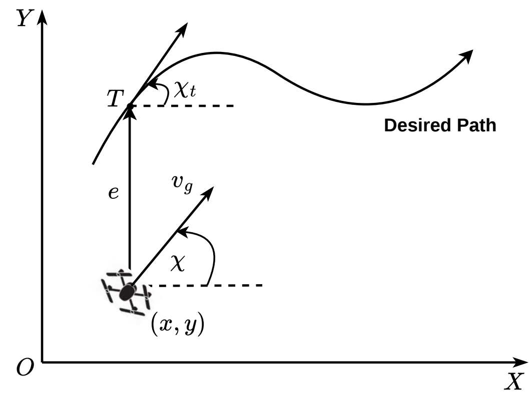

Fig. 2: Geometry of the curvilinear path-following problem

III. PROPOSED GUIDANCE LAW

This section presents a VF guidance strategy for accurately following curvilinear paths. Let the desired path be represented as $y = f(x)$. The tracking error e is defined as the vertical deviation of the UAV from the desired path and illustrated in Fig. 2, is given by

$$e = f(x) - y. \tag{4}$$

Let T denote the corresponding point on the desired path. The course angle of the path at point T is given by

$$\chi_t = \tan^{-1}\left(\frac{dy}{dx}\right) \tag{5}$$

where, $\chi_t \in (-\pi/2, \pi/2)$. The rate of change of the tracking error in (4) is obtained as

$$\begin{aligned} \dot{e} &= \frac{df(x)}{dt} - \frac{dy}{dt} \\ &= \frac{df(x)}{dx}\frac{dx}{dt} - \frac{dy}{dt} \\ &= \tan(\chi_t) v_g \cos(\chi) - v_g \sin(\chi) \\ &= v_g \frac{\sin(\chi_t - \chi)}{\cos(\chi_t)} \end{aligned} \tag{6}$$

The objective is to design the vector field such that, as the tracking error $e \to 0$, the course angle χ converges to χ_t, ensuring alignment of the UAV with the desired path. To achieve this objective, the desired course vector field is defined as

$$\chi_d = \begin{cases} \chi_t - \frac{\pi}{2} + \cos^{-1}(1 - \exp(ke)), & e \leq 0 \\ \chi_t + \frac{\pi}{2} - \cos^{-1}(1 - \exp(-ke)), & e > 0 \end{cases} \tag{7}$$

where k is a positive constant that governs the convergence behavior. The desired course angle χ_d is defined relative to the path tangent direction χ_t and varies continuously with respect to the tracking error $e \in (-\infty, \infty)$. In particular, as $e \to 0$, $\chi_d \to \chi_t$, ensuring alignment with the desired path. For large tracking errors, i.e., $e \gg 0$, $\chi_d \to \chi_t + \frac{\pi}{2}$, and for $e \ll 0$, $\chi_d \to \chi_t - \frac{\pi}{2}$, ensuring convergence toward the desired path. Furthermore, larger values of k result in sharper transitions near the path, whereas smaller values yield smoother convergence.

Proposition 1. In accordance with the desired course angle χ_d defined in (7), the tracking error e asymptotically converges to zero for any initial condition.

Proof. Consider the Lyapunov candidate $V_1(e) = \frac{1}{2}e^2$, which is positive definite and radially unbounded. Time derivative of $V_1(e)$ is given by

$$\dot{V}_1(e) = e\dot{e}. \tag{8}$$

Using the error dynamics in (6), and assuming $\chi = \chi_d$, we obtain

$$\dot{V}_1(e) = ev_g \frac{\sin(\chi_t - \chi_d)}{\cos(\chi_t)}. \tag{9}$$

Substituting the desired course angle from (7), (9) reduces to

$$\dot{V}_1(e) = -|e|\, v_g \frac{1-\exp(-k|e|)}{\cos(\chi_t)} \tag{10}$$

Since $\chi_t \in (-\pi/2, \pi/2)$, it follows that $\cos\chi_t > 0$. Furthermore, $(1-\exp(ke)) \geq 0$ for $e \leq 0$ and $(1-\exp(-ke)) \geq 0$ for $e > 0$. Hence,

$$\dot{V}_1(e) < 0, \quad \forall e \neq 0, \quad \text{and} \quad \dot{V}_1(e) = 0, \quad \text{for} \quad e = 0. \tag{11}$$

Therefore, $\dot{V}_1(e)$ is negative definite, and the equilibrium point $e = 0$ is asymptotically stable. Consequently, the tracking error e asymptotically converges to zero. ■

Define the manifold $\mathscr{S} = \{(e,\chi) \mid \chi = \chi_d(e)\}$. A sliding mode control law is designed to ensure that the system trajectories reach $\mathscr{S}$ in finite time. Define the course angle tracking error as $\tilde{\chi} = \chi - \chi_d$. Taking the time derivative yields

$$\dot{\tilde{\chi}} = \alpha(\chi_c - \chi) - \dot{\chi}_d \tag{12}$$

Using (6) and (7), $\dot{\chi}_d$ is written as

$$\dot{\chi}_d = \dot{\chi}_t + \frac{k\exp(-k|e|)}{\sqrt{1-(1-\exp(-k|e|))^2}} \frac{v_g \sin(\chi_t - \chi)}{\cos(\chi_t)} \tag{13}$$

Substituting (13) into (12), results in

$$\dot{\tilde{\chi}} = \alpha(\chi_c - \chi) - \dot{\chi}_t - \frac{k\exp(-k|e|)}{\sqrt{1-(1-\exp(-k|e|))^2}} \frac{v_g \sin(\chi_t - \chi)}{\cos(\chi_t)} \tag{14}$$

Consider the Lyapunov candidate $V_2 = \frac{1}{2}\tilde{\chi}^2$. Time derivative of V_2 gives

$$\dot{V}_2 = \tilde{\chi}\Big(\alpha(\chi_c - \chi) - \dot{\chi}_t - \frac{k\exp(-k|e|)}{\sqrt{1-(1-\exp(-k|e|))^2}} \frac{v_g \sin(\chi_t - \chi)}{\cos(\chi_t)}\Big) \tag{15}$$

Since the desired path is known, the derivative of the path course angle $\dot{\chi}_t$ can be computed and incorporated into the control input. With an appropriate control design, substitution into the Lyapunov derivative $\dot{V}_2$ eliminates this term. Thus, the commanded course χ_c is chosen as

$$\chi_c = \chi + \frac{\dot{\chi}_t}{\alpha} + \frac{v_g}{\alpha} \frac{k\exp(-k|e|)}{\sqrt{1-(1-\exp(-k|e|))^2}} \frac{\sin(\chi_t - \chi)}{\cos(\chi_t)} - \frac{\eta}{\alpha}\operatorname{sign}(\tilde{\chi}) \tag{16}$$

where,

$$\operatorname{sign}(z) = \begin{cases} 1, & \text{if } z > 0 \\ 0, & \text{if } z = 0 \\ -1, & \text{if } z < 0 \end{cases} \tag{17}$$

and $\eta > 0$. Then,

$$\dot{V}_2 \leq -\eta\, |\tilde{\chi}|\,. \tag{18}$$

which ensures finite-time reachability of the sliding manifold $\mathscr{S}$.

However, the discontinuous nature of the sign function may induce chattering. To mitigate this effect, the commanded course in (16) is modified as

$$\chi_c = \chi + \frac{\dot{\chi}_t}{\alpha} + \frac{v_g}{\alpha} \frac{k\exp(-k|e|)}{\sqrt{1-(1-\exp(-k|e|))^2}} \frac{\sin(\chi_t - \chi)}{\cos(\chi_t)} - \frac{\eta}{\alpha}\operatorname{sat}\left(\frac{\tilde{\chi}}{\varepsilon}\right) \tag{19}$$

where,

$$\operatorname{sat}(z) = \begin{cases} z, & \text{if, } |z| \leq 1 \\ \operatorname{sign}(z), & \text{otherwise} \end{cases} \tag{20}$$

The characteristics of the sliding surface and the corresponding system trajectories are governed by the control parameters k, η and ε. Here, k controls the steepness of the sliding surface near the origin, η influences the convergence rate of the state trajectory, and ε defines the width of the transition region around the sliding surface.

Theorem 1. Consider the UAV kinematics described by (2) and the course error dynamics in (14). Under the commanded course defined in (19), the system is globally asymptotically stable.

Proof. Define the Lyapunov candidate function as

$$V = \frac{1}{2}e^2 + \frac{1}{2}\mu\tilde{\chi}^2, \quad \mu > 0. \tag{21}$$

The function V is positive definite and satisfies

$$V \geq \frac{1}{2}\min\{1,\mu\}(e^2 + \tilde{\chi}^2), \tag{22}$$

which implies that V is radially unbounded. The time derivative of V is given by

$$\dot{V} = e\dot{e} + \mu\tilde{\chi}\dot{\tilde{\chi}}. \tag{23}$$

Substituting (2), (14) and (19) into (23) yields

$$\begin{aligned} \dot{V} &= e\dot{e} - \mu\eta\operatorname{sat}\left(\frac{\tilde{\chi}}{\varepsilon}\right)\tilde{\chi} \\ &= \begin{cases} e\dot{e} - \frac{\mu\eta}{\varepsilon}\tilde{\chi}^2, & |\tilde{\chi}| < \varepsilon, \\ e\dot{e} - \frac{\mu\eta}{\varepsilon}|\tilde{\chi}|, & |\tilde{\chi}| \geq \varepsilon. \end{cases} \end{aligned} \tag{24}$$

From Proposition 1, it follows that $e\dot{e} < 0$ for all $e \neq 0$. Furthermore, the terms $-\frac{\mu\eta}{\varepsilon}\tilde{\chi}^2$ and $-\frac{\mu\eta}{\varepsilon}|\tilde{\chi}|$ are strictly negative for $\tilde{\chi} \neq 0$. Hence, $\dot{V} < 0$ for all $(e, \tilde{\chi}) \neq (0,0)$. Since V is positive definite and radially unbounded, and $\dot{V}$ is negative definite, the equilibrium $(e, \tilde{\chi}) = (0,0)$ is globally asymptotically stable. ■

IV. SIMULATION RESULTS

The proposed guidance framework is validated through numerical simulations performed in MATLAB R2023a. Two representative curvilinear paths are considered: a parabolic path and a cubic polynomial path. The UAV airspeed is maintained at $v_a = 10$ m/s. A steady wind disturbance with magnitude $v_w = 5$ m/s and direction $\psi_w = 30°$ is incorporated. The guidance parameters in (19) are selected as $k = 0.12$, $\eta = 1$, and $\varepsilon = 1$.

A. Parabolic Path Following

The desired path is defined as $y = 0.008x^2$. Two initial conditions are considered to evaluate the effectiveness of the proposed guidance law: **Case 1:** $(x_i, y_i) = (-100, -20)$ m with $\chi_0 = 90°$, and **Case 2:** $(x_i, y_i) = (-100, 125)$ m with $\chi_0 = 0°$. Fig. 3(a) shows that the UAV converges to the desired path in both cases. The corresponding course angle evolution is presented in Fig. 3(b), exhibiting smooth transient behavior. The tracking error response in Fig. 3(c) confirms convergence to zero. Fig. 3(d) presents the lateral acceleration profiles, computed as $a_u = v_g\dot{\chi}$, which remain smooth.

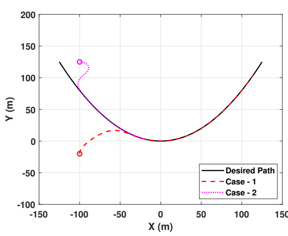

(a) UAV trajectory

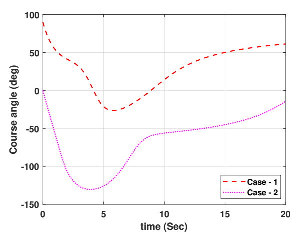

(b) Course angle

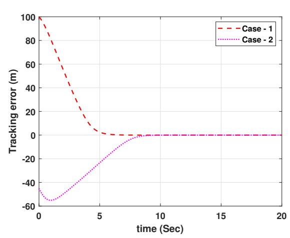

(c) Tracking error

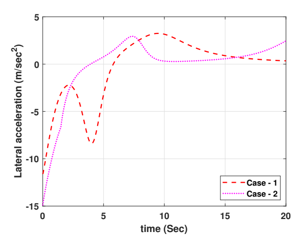

(d) Lateral acceleration

Fig. 3: Results for parabolic path following

B. Polynomial Path Following

In this scenario, the desired path is defined as $y = 0.0005x^3 - 0.05x^2 + 0.5x$. Similar to parabolic path following, two initial conditions are considered: **Case 1:** $(x_i, y_i) = (0, -50)$ m with $\chi_0 = 90°$, and **Case 2:** $(x_i, y_i) = (0, 50)$ m with $\chi_0 = 0°$. Fig. 4(a) shows the UAV trajectories for both cases, which demonstrate accurate path following. The corresponding course angle profiles are presented in Fig. 4(b). The tracking error response in Fig. 4(c) shows that the error converges to zero, which further confirms precise path following. Furthermore, Fig. 4(d) presents the lateral acceleration profiles for both cases.

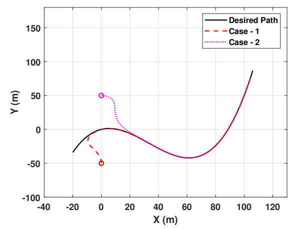

(a) UAV trajectory

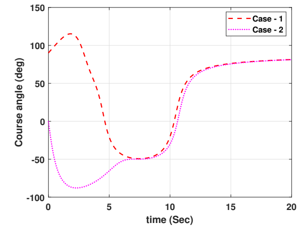

(b) Course angle

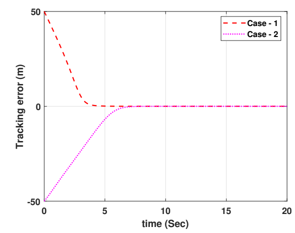

(c) Tracking error

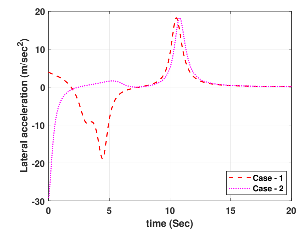

(d) Lateral acceleration

Fig. 4: Results for polynomial path following

V. COMPARATIVE STUDY

In this section, the proposed VF guidance framework is compared with two existing VF guidance algorithms, namely the guidance laws in [11] and [19], in the presence of steady wind. The desired path for comparison is defined as $y = 10\sin(0.05x)$. The UAV starts from the initial position $(-100, -20)$ m with an initial orientation of 90°, maintaining a constant airspeed of 10 m/s. The wind velocity magnitude and direction are set to 5 m/s and 30°, respectively. The control parameters for the proposed guidance law are kept the same as those used in the simulation section, whereas the parameters for the existing guidance laws are selected as reported in the respective literature. The VF gain for all guidance laws is set to $k = 0.12$.

The comparison is based on two performance metrics: settling time and total control effort. The settling time is defined as the time required for the lateral deviation to enter and remain within ± 0.2 m of the desired path, while the total control effort is defined as $\int_0^t a_u^2\, dt$. The comparative results are summarized in TABLE I, and the corresponding responses are shown in Fig. 5. The trajectories of all guidance algorithms are presented in Fig. 5(a), while the course angle responses are shown in Fig. 5(b). The tracking error responses are illustrated in Fig. 5(c), where the zoomed view shows that the guidance law in [19] exhibits a small overshoot, whereas the other two guidance laws converge to zero without overshoot for the selected gain. The lateral acceleration histories are presented in Fig. 5(d). From TABLE I, it is evident that the proposed guidance law achieves lower control effort compared to the guidance laws in [11] and [19]. Overall, the results highlight the superiority of the proposed guidance framework in terms of tracking performance and control efficiency under wind disturbances.

TABLE I: Comparative Performance of Guidance Laws

Guidance Method	**Settling Time (s)**	**Control Effort** ($\mathrm{m}^2/\mathrm{s}^3$)
Proposed	4.24	342.5
Nelson et al. [11]	4.11	1560.8
Shivam et al. [19]	4.63	1121.1

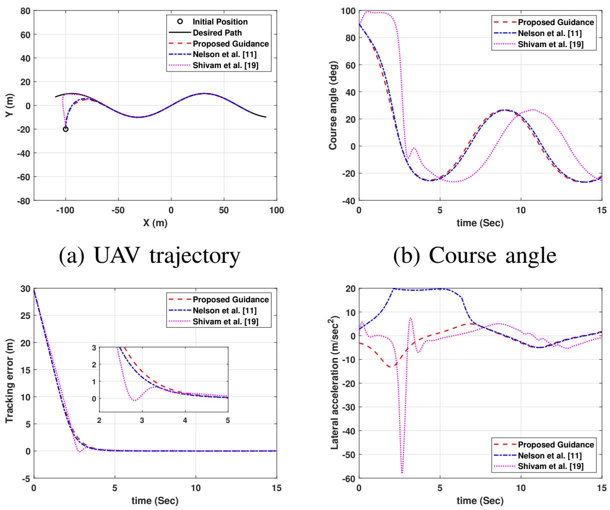

(a) UAV trajectory (b) Course angle

(c) Tracking error (d) Lateral acceleration

Fig. 5: Comparisons with existing guidance laws

VI. EXPERIMENTAL RESULTS

Experimental validation of the proposed guidance strategy was performed using a Quanser QDrone platform within an indoor laboratory setting. The experimental infrastructure consisted of a motion capture system and a desktop-based ground station. State estimation was achieved using a network of six OptiTrack Flex 13 cameras, providing high-frequency and accurate position measurements. The guidance algorithm generated waypoint commands, which were transmitted to the onboard processor of the quadrotor via a WiFi communication link. These reference waypoints, together with real-time pose information, were utilized by the onboard controller to compute the required control inputs, namely thrust and body moments, which were subsequently converted into rotor speed commands for trajectory tracking.

The experimental study focused on a sinusoidal path-following task. The quadrotor was operated at a constant altitude of 0.8 m and maintained a speed of 0.3 m/s. The desired trajectory was defined as $y = 0.8\sin(\pi x)$, with the vehicle initialized at position $(-1,-1)$ m and an initial orientation of $0°$. As illustrated in Fig. 6(a), the reference trajectory generated by the guidance law (blue) and the actual flight trajectory (red) show close agreement. The time histories of the X, Y, and Z positions are presented in Figs. 6(b)–(d), respectively, while the desired and measured yaw angles are compared in Fig. 6(e). The results depicted in Fig. 6 demonstrate satisfactory tracking accuracy, thereby confirming the practical effectiveness of the proposed guidance approach in real-time flight experiments.

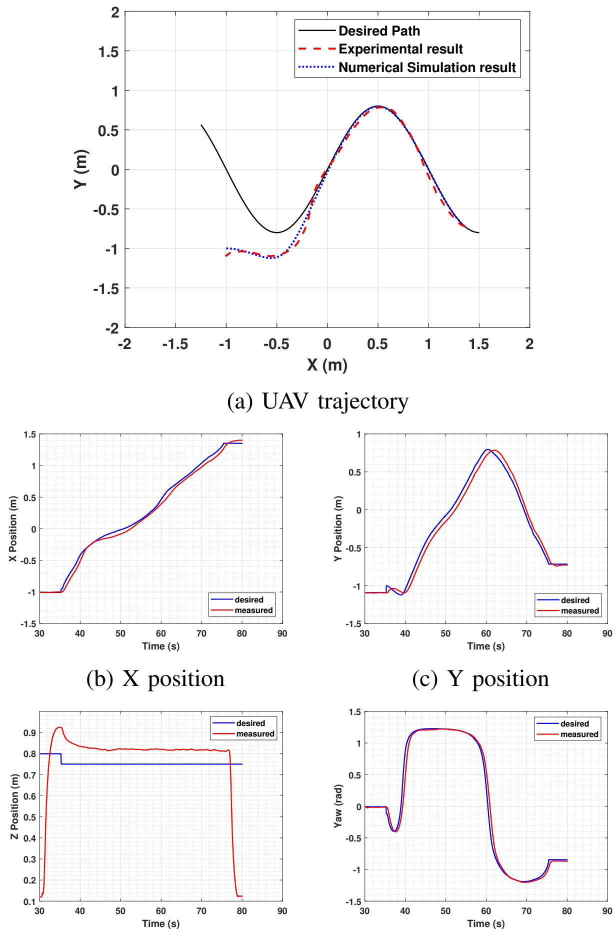

(a) UAV trajectory

(b) X position (c) Y position

(d) Z position (e) Yaw

Fig. 6: Experimental results for trajectory tracking

VII. CONCLUSION

This paper presents a VF-based guidance framework for accurate path following of curvilinear paths. The approach employs an arccosine-based formulation to generate the desired course angle, while a SMC strategy is utilized to design the commanded course angle and ensure finite-time convergence of the course-angle error. Numerical simulations on various curvilinear paths demonstrate the robustness and effectiveness of the guidance strategy under steady wind conditions. Comparative evaluations with existing guidance methods indicate improved performance with reduced control effort. These results highlight its potential for enhancing UAV path-following capability. Experimental results further validate the practical applicability of the framework and demonstrate accurate trajectory tracking under real-world operating conditions. Future work focuses on extending the framework to three-dimensional environments and addressing path-following challenges in cluttered scenarios.

REFERENCES

[1] X. Jin, W. Mei, and Y. Zhaolong, "Path following control for unmanned aerial vehicle based on carrot chasing algorithm and PLOS," in *2020 IEEE International Conference on Artificial Intelligence and Information Systems (ICAIIS)*. IEEE, 2020, pp. 571–576.

[2] T. Yamasaki, H. Takano, and Y. Baba, "Robust path-following for UAV using pure pursuit guidance," in *Aerial Vehicles*. IntechOpen, 2009.

[3] R. Rysdyk, "UAV path following for constant line-of-sight," in *2nd AIAA" Unmanned Unlimited" Conf. and Workshop & Exhibit*, 2003, p. 6626.

[4] S. Park, J. Deyst, and J. How, "A new nonlinear guidance logic for trajectory tracking," in *AIAA guidance, navigation, and control conference and exhibit*, 2004, p. 4900.

[5] A. Ratnoo, S. Y. Hayoun, A. Granot, and T. Shima, "Path following using trajectory shaping guidance," *Journal of Guidance, Control, and Dynamics*, vol. 38, no. 1, pp. 106–116, 2015.

[6] M. Z. Shah, R. Samar, and A. I. Bhatti, "Guidance of air vehicles: A sliding mode approach," *IEEE Transactions on Control Systems Technology*, vol. 23, no. 1, pp. 231–244, 2014.

[7] H. Bouadi, M. Bouchoucha, and M. Tadjine, "Sliding mode control based on backstepping approach for an UAV type-quadrotor," *World Academy of Science, Engineering and Technology*, vol. 26, no. 5, pp. 22–27, 2007.

[8] S. Kukreti, M. Kumar, and K. Cohen, "Genetically tuned lqr based path following for UAVs under wind disturbance," in *2016 International Conference on Unmanned Aircraft Systems (ICUAS)*. IEEE, 2016, pp. 267–274.

[9] S. Pal and S. Hota, "Nonlinear control law for path following by UAVs," in *2024 Tenth Indian Control Conference (ICC)*. IEEE, 2024, pp. 476–481.

[10] P. Sujit, S. Saripalli, and J. B. Sousa, "Unmanned aerial vehicle path following: A survey and analysis of algorithms for fixed-wing unmanned aerial vehicles," *IEEE Control Systems Magazine*, vol. 34, no. 1, pp. 42–59, 2014.

[11] D. R. Nelson, D. B. Barber, T. W. McLain, and R. W. Beard, "Vector field path following for miniature air vehicles," *IEEE Transactions on Robotics*, vol. 23, no. 3, pp. 519–529, 2007.

[12] S. Griffiths, "Vector field approach for curved path following for miniature aerial vehicles," in *AIAA guidance, navigation, and control conference and exhibit*, 2006, p. 6467.

[13] X. Wang, S. Roy, S. Fari, and S. Baldi, "Adaptive vector field guidance without a priori knowledge of course dynamics and wind," *IEEE/ASME Transactions on Mechatronics*, vol. 27, no. 6, pp. 4597–4607, 2022.

[14] S. Pal and S. Hota, "Vector field guidance with curvature constraint for UAVs," in *AIAA SCITECH 2025 Forum*, 2025, p. 0523.

[15] D. Lawrence, "Lyapunov vector fields for UAV flock coordination," in *2nd AIAA" Unmanned Unlimited" Conf. and Workshop & Exhibit*, 2003, p. 6575.

[16] D. Lawrence, E. Frew, and W. Pisano, "Lyapunov vector fields for autonomous UAV flight control," in *AIAA Guidance, Navigation and Control Conference and Exhibit*, 2007, p. 6317.

[17] A. A. Pothen and A. Ratnoo, "Curvature-constrained lyapunov vector field for standoff target tracking," *Journal of Guidance, Control, and Dynamics*, vol. 40, no. 10, pp. 2729–2736, 2017.

[18] T. Harinarayana, S. Hota, and R. Kushwaha, "Vector field guidance for standoff target tracking," *Proceedings of the Institution of Mechanical Engineers, Part G: Journal of Aerospace Engineering*, vol. 236, no. 14, pp. 2963–2973, 2022.

[19] A. Shivam and A. Ratnoo, "Arcsine vector field for path following guidance," *Journal of Guidance, Control, and Dynamics*, vol. 46, no. 12, pp. 2409–2420, 2023.

[20] S. Pal and S. Hota, "Curvature constrained vector field guidance for UAVs," *IEEE Transactions on Aerospace and Electronic Systems*, pp. 1–13, 2026.